

Sensitivity of Southern Ocean overturning to wind stress changes: Role of surface restoring time scales

Xiaoming Zhai^{a,*}, David R. Munday^b

^a*Centre for Ocean and Atmospheric Sciences, School of Environmental Sciences,
University of East Anglia, Norwich, UK*

^b*Atmospheric, Oceanic and Planetary Physics, Department of Physics, University of
Oxford, Oxford, UK*

Abstract

The influence of different surface restoring time scales on the response of the Southern Ocean overturning circulation to wind stress changes is investigated using an idealised channel model. Regardless of the restoring time scales chosen, the eddy-induced meridional overturning circulation (MOC) is found to compensate for changes of the direct wind-driven Eulerian-mean MOC, rendering the residual MOC less sensitive to wind stress changes. However, the extent of this compensation depends strongly on the restoring time scale: residual MOC sensitivity increases with decreasing restoring time scale. Strong surface restoring is shown to limit the ability of the eddy-induced MOC to change in response to wind stress changes and as such suppresses the eddy compensation effect. These model results are consistent with qualitative arguments derived from residual-mean theory and may have important implications for interpreting past and future observations.

Keywords: Surface restoring, Southern Ocean, Ocean eddies, Meridional

*Corresponding author

Email address: xiaoming.zhai@uea.ac.uk (Xiaoming Zhai)

1. Introduction

Upwelling in the Southern Ocean, driven by the prevailing westerly winds, plays a key role in closing the Meridional Overturning Circulation (MOC) of the global ocean (e.g. Marshall and Speer, 2012). Changes of the strength of this upwelling branch of the MOC associated with changes of the Southern Ocean winds have been proposed as an important mechanism for regulating global climate, in particular, through enhancing or reducing the communication between the carbon-rich deep ocean and the surface (e.g. Toggweiler and Russell, 2008; Anderson et al., 2009). Projections from state-of-the-art climate models suggest that the Southern Ocean westerlies are likely to strengthen as well as become stormier over the next few decades (e.g. Solomon et al., 2007; Chang et al., 2012), both of which act to enhance the Southern Ocean surface wind stress (e.g. Zhai et al., 2012; Zhai, 2013). However, the robust response of the Southern Ocean overturning circulation to changes of the wind field is yet to be determined.

The problem of how the Southern Ocean responds to changes in surface wind stress has been investigated previously in both ocean-only and coupled general circulation models (e.g. Fyfe and Saenko, 2006; Hallberg and Gnanadesikan, 2006; Meredith and Hogg, 2006; Farneti et al., 2010; Viebahn and Eden, 2010; Abernathey et al., 2011; Meredith et al., 2012; Munday et al., 2013). Models that resolve mesoscale ocean eddies are generally found to be less sensitive to wind stress changes than those with parameterised ed-

23 dies in terms of both circumpolar volume transport/global pycnocline depth
24 and MOC. This insensitivity comes from the subtle balance between the
25 wind-driven Eulerian-mean MOC that acts to steepen isopycnals and the
26 eddy-induced MOC that acts to flatten them out; this balance largely de-
27 termines the net residual MOC in the Southern Ocean (e.g. Marshall, 1997).
28 Note that it is the residual circulation that advects temperature, salinity,
29 CO₂ and other climatically-important tracers in the eddying ocean.

30 In eddy-resolving ocean models, an increase in the Southern Ocean wind
31 stress results in enhanced Ekman divergence and convergence that acts to
32 tilt the isopycnals further and increase the mean available potential en-
33 ergy (APE) of the system. This leads to the generation of a more vigor-
34 ous eddy field that releases the newly-increased APE and at least partially
35 compensates for changes of the wind-driven overturning. As a result, the
36 residual MOC is rendered less sensitive to changes of wind stress, that is,
37 changes of the residual MOC are much smaller than those of the direct wind-
38 driven Eulerian-mean MOC (the so-called *eddy compensation* effect; Viebahn
39 and Eden (2010)). It is, however, unlikely to have perfect eddy compensa-
40 tion due to the different depth dependence of the Ekman and eddy-induced
41 transports; changes of the Ekman transport are strongly surface-intensified
42 whereas changes of the eddy-induced transport spread over the whole water
43 depth (e.g. Morrison and Hogg, 2013).

44 The extent to which changes in the eddy-induced MOC compensate for
45 changes in the wind-driven Eulerian-mean MOC varies among different eddy-
46 resolving models. For example, relatively weak sensitivity of the residual
47 MOC to altered wind forcing is found in an eddying model of Hallberg

48 and Gnanadesikan (2006), while greater sensitivity is found in the models of
 49 Viebahn and Eden (2010) and Munday et al. (2013). Recently, Abernathey
 50 et al. (2011) showed that the sensitivity of the Southern Ocean residual MOC
 51 to changes of the wind forcing depends on the surface boundary condition for
 52 buoyancy: a fixed surface buoyancy flux boundary condition severely limits
 53 the ability of the residual MOC to change, whereas the use of a Haney-type
 54 restoring boundary condition for buoyancy (Haney, 1971) leads to greater
 55 sensitivity. Since in thermodynamic equilibrium the residual MOC matches
 56 the buoyancy forcing (e.g. Walin, 1982; Watson and Naveira Garabato, 2006;
 57 Badin and Williams, 2010), the higher degree of freedom at which surface
 58 buoyancy flux can vary under the restoring boundary condition implies a
 59 higher sensitivity of the residual MOC.

60 In Abernathey et al. (2011), a surface restoring time scale of 30 days
 61 was used for model experiments under the restoring boundary condition. In
 62 the ocean, due to the lack of observations, it remains unclear on what time
 63 scales the surface turbulent heat fluxes damp the sea surface temperature
 64 anomalies, although the spatial scales of these anomalies are believed to be
 65 important (e.g. Bretherton, 1982; Frankignoul, 1985)¹. For example, studies
 66 based on heat flux data derived from ship and satellite observations suggest
 67 that the restoring time scales can vary from less than one month to almost
 68 one year in the Southern Ocean, depending on season and location (e.g. Park
 69 et al., 2005). Recently, Shuckburgh et al. (2011) studied the mixed layer lat-

¹The situation for the sea surface salinity (SSS) is very different because it does not
 rain preferentially over regions of positive SSS anomalies nor evaporate preferentially over
 regions of negative SSS anomalies (e.g. Zhai and Greatbatch, 2006a,b)

70 eral eddy fluxes mediated by air-sea interaction and found a large sensitivity
71 of surface eddy diffusivity to prescribed surface restoring time scale. How-
72 ever, the question of whether and how the sensitivity of the Southern Ocean
73 MOC to changes in wind stress depends on the surface restoring time scale
74 is, to our knowledge, yet to be explored.

75 The aim of this study is to investigate the effect of different surface restor-
76 ing time scales on the response of the Southern Ocean overturning to wind
77 stress changes, extending the recent work by Abernathey et al. (2011). We
78 begin in Section 2 by presenting some qualitative arguments based on the
79 residual-mean framework of Marshall and Radko (2003) to illustrate the in-
80 fluence of different surface boundary conditions. After describing the numer-
81 ical model setup and experiment design in Section 3, we present and discuss
82 changes of the eddy-induced and residual MOCs in response to wind stress
83 changes in experiments with various restoring time scales in Section 4. We
84 close with a summary in Section 5.

85 **2. Role of surface restoring on Southern Ocean response**

86 Here we adopt the residual-mean framework of Marshall and Radko (2003)
87 to illustrate the influence of different surface restoring time scales on the re-
88 sponse of the Southern Ocean to wind stress changes. The time and zonally-
89 averaged buoyancy equation is given by

$$J(\Psi_{res}, \bar{b}) = \frac{\partial \bar{B}}{\partial z}, \quad (1)$$

90 where $b = -g(\rho - \rho_0)/\rho_0$ is buoyancy, B is the buoyancy forcing, Ψ_{res} is the
91 streamfunction of the residual circulation in the meridional plane (MOC),

92 and overbars denote time and zonal averaging. Following Marshall and Radko
 93 (2003), the residual MOC can be written as a combination of the Eulerian-
 94 mean MOC ($\bar{\Psi}$) and the eddy-induced MOC (Ψ^*), i.e.

$$\Psi_{res} = \bar{\Psi} + \Psi^* = -\frac{\tau}{\rho_0 f} + K s, \quad (2)$$

95 where τ is zonal wind stress, ρ_0 is reference density, f is the Coriolis param-
 96 eter, $s = -\bar{b}_y/\bar{b}_z$ is the mean isopycnal slope and K is the eddy thickness
 97 diffusivity.

98 Using mixing length theory, the eddy diffusivity can be expressed as

$$K \simeq V_e L_e, \quad (3)$$

99 where V_e denotes a characteristic eddy velocity and L_e denotes a character-
 100 istic eddy length scale. Following Visbeck et al. (1997) and Marshall et al.
 101 (2012), we assume that $V_e \simeq \sigma L_e$, where σ is the Eady growth rate, given by

$$\sigma = \frac{f}{\sqrt{Ri}} = \frac{f}{N/|\bar{u}_z|} = N|s|. \quad (4)$$

102 Here N is the buoyancy frequency with $N^2 = \bar{b}_z$. Eq. (4) shows that the
 103 eddy growth rate depends linearly on the mean isopycnal slope. Combining
 104 Eqs. (2), (3) and (4), while noting that s is always negative in our model
 105 (see Fig. 1), the eddy diffusivity is then given by

$$K \simeq -L_e^2 N s, \quad (5)$$

106 and the eddy-induced MOC is given by

$$\Psi^* \simeq -L_e^2 N s^2. \quad (6)$$

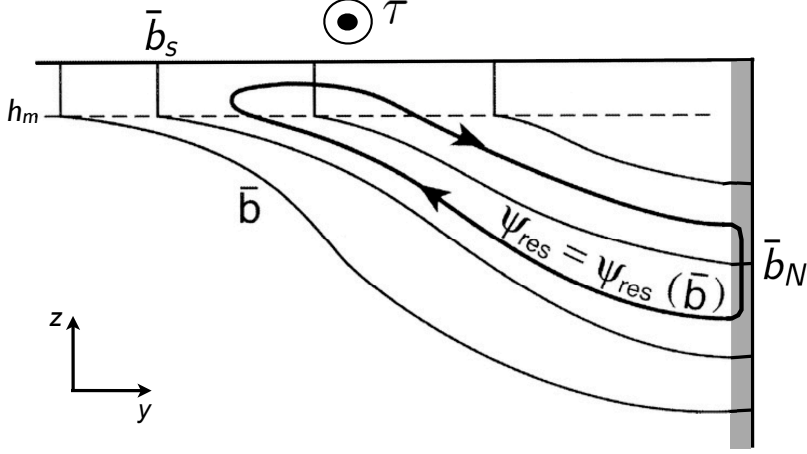


Figure 1: Schematic of the conceptual model (modified from Marshall and Radko (2003)). The residual MOC is directed along the mean isopycnals in the ocean interior and closed by diapycnal circulation in the surface diabatic and northern sponge layers. The northern sponge layer is shaded in grey.

107 The eddy-induced MOC is therefore anticlockwise and depends quadratically
 108 on the mean isopycnal slope (e.g. Visbeck et al., 1997).

109 Following Marshall and Radko (2003), we assume zero stratification within
 110 the surface mixed layer and neglect the entrainment fluxes at its base. In-
 111 tegrating Eq. (1) over the depth of the surface mixed layer h_m while noting
 112 $\Psi_{res} = 0$ at the surface gives

$$\Psi_{res}|_{z=-h_m} \frac{\partial \bar{b}_s}{\partial y} = \bar{B}, \quad (7)$$

113 where \bar{B} is interpreted as the effective buoyancy forcing that includes both
 114 air-sea buoyancy fluxes and lateral diabatic eddy fluxes in the mixed layer.

115 In the ocean interior, we assume the buoyancy forcing is weak, i.e., $B = 0$,
 116 and Eq. (1) reduces to

$$J(\Psi_{res}, \bar{b}) = 0, \quad (8)$$

117 meaning that the residual circulation remains constant along the mean isopy-
 118 cnals, i.e., $\Psi_{res} = \Psi_{res}(\bar{b})$.

119 At the northern boundary of our model, the buoyancy distribution through-
 120 out the water column is prescribed through a restoring boundary condition
 121 at a short time scale, i.e.,

$$\bar{b} = \bar{b}_N(z). \quad (9)$$

122 Physically, \bar{b}_N is set by ocean adjustment to global diabatic processes further
 123 to the north of our model domain (Munday et al., 2011). Figure 1 shows
 124 a schematic of the conceptual model used by this study. We now consider
 125 surface restoring boundary conditions at two limits.

126 *2.1. Strong surface restoring*

127 In the limit of strong surface restoring ($\lambda \gg \sigma$, where λ^{-1} is the surface
 128 restoring time scale), buoyancy at the surface, b_s , is effectively prescribed,
 129 leaving the isopycnal slopes little freedom to vary. Since the eddy-induced
 130 MOC is, to a large extent, determined by the isopycnal slopes (see Eq. (6)),
 131 changes of the eddy-induced MOC, and therefore the ability of eddies to
 132 compensate for wind stress changes, is severely suppressed. As a result, the
 133 residual MOC exhibits a large sensitivity to changes of the wind forcing, with
 134 changes of the residual MOC, $\Delta\Psi_{res}$, approaching that of the Eulerian-mean
 135 MOC, $\Delta\bar{\Psi}$, i.e.,

$$\Delta\Psi_{res} \sim \Delta\bar{\Psi} = -\frac{\Delta\tau}{\rho_0 f}. \quad (10)$$

136 Changes in the effective buoyancy forcing associated with changes in wind
 137 stress can be approximated by

$$\Delta\bar{B} \sim -\frac{\Delta\tau}{\rho_0 f} \frac{\partial \bar{b}_s}{\partial y}. \quad (11)$$

138 Physically, in the strong surface restoring limit, stronger surface Ekman flow
 139 driven by increased wind stress crosses the mean isopycnals in the mixed
 140 layer experiencing swift water mass transformation due to the efficient surface
 141 restoring buoyancy flux. As a result, the isopycnals do not alter their mean
 142 slope. This is the diabatic surface Ekman drift situation.

143 The mean APE of the ocean is proportional to the mean isopycnal slope
 144 squared (Smith, 2007). It follows that the surface restoring boundary condi-
 145 tion acts as a source of mean APE by preventing the isopycnals from slump-
 146 ing when the wind stress weakens. However, it acts as a sink for the mean
 147 APE by preventing the isopycnals from further steepening when the wind
 148 stress strengthens. This is particularly clear in the case of our numerical
 149 experiments without surface wind stress forcing (see Section 4).

150 2.2. Weak surface restoring

151 In the limit of weak or no surface restoring ($\lambda \ll \sigma$; no restoring, i.e.,
 152 $\lambda^{-1} = \text{infinity}$, corresponds to a fixed surface buoyancy flux), b_s at the surface
 153 is free to change, while being related to b_N at the model northern boundary
 154 via the isopycnal slope s ,

$$\bar{b}_s(y) = \bar{b}_N(z = -ys), \quad (12)$$

155 with

$$\frac{\partial \bar{b}_s}{\partial y} = -s \frac{\partial \bar{b}_N}{\partial z}, \quad (13)$$

156 if we assume s is uniform. Eq. (7) can now be rewritten as

$$\left(\frac{\tau}{\rho_0 f} s - K s^2 \right) \frac{\partial \bar{b}_N}{\partial z} = \bar{B}, \quad (14)$$

157 which can be solved either analytically or numerically for s for given τ , \bar{b}_N
 158 and \bar{B} . Note that \bar{B} includes not only air-sea buoyancy fluxes but also lateral
 159 diabatic eddy transfer in the mixed layer. Although air-sea buoyancy fluxes
 160 are more or less fixed in the weak surface restoring limit, the diabatic eddy
 161 fluxes in the mixed layer may still change in response to changes of wind
 162 stress. If we assume the overall changes of \bar{B} are small in the weak surface
 163 restoring limit (see also Abernathey et al., 2011), it then follows from Eq. (14)
 164 that the isopycnal slope s (and hence the eddy-induced MOC) must change
 165 in response to changes in wind stress. Stronger Ekman flow advects the mean
 166 isopycnals in the mixed layer and tilts the isopycnals further, leading to a
 167 stronger eddy field that acts to shift the mean isopycnals back.

168 Assuming that the isopycnal slope increases from s to $s + \Delta s$ in response
 169 to wind stress changes from τ to $\tau + \Delta\tau$, the eddy diffusivity then increases
 170 from K to $K + \Delta K$ with $\Delta K = -L_e^2 N \Delta s$. Substituting these into Eq. (14)
 171 and neglecting higher order Δs terms, we obtain

$$\Delta s = \frac{-\frac{\Delta\tau}{\rho_0 f}}{3L_e^2 N s^2 + \frac{\tau}{\rho_0 f}} s. \quad (15)$$

172 Changes of the residual circulation Ψ_{res} is given by

$$\Delta\Psi_{res} = -\frac{\Delta\tau}{\rho_0 f} + K\Delta s + s\Delta K, \quad (16)$$

173 where the quadratic $\Delta s\Delta K$ term has been dropped. After some simple
 174 algebra, we find

$$\Delta\Psi_{res} = -\frac{\Delta\tau}{\rho_0 f} \frac{L_e^2 N s^2 + \frac{\tau}{\rho_0 f}}{3L_e^2 N s^2 + \frac{\tau}{\rho_0 f}} \approx -\frac{\Delta\tau}{\rho_0 f} \left(\frac{\Psi_{res}}{2\Psi^*} \right). \quad (17)$$

175 The key point here is that although $\Delta\Psi_{res}$ still scales linearly with changes
 176 of wind stress, the slope is much reduced in comparison with Eq. (10) since

177 $|\Psi_{res}| \ll |2\Psi^*|^2$. This result means that the residual circulation is much less
 178 sensitive to wind stress changes in the weak surface restoring limit than in
 179 the strong surface restoring limit.

180 **3. Numerical model experiment**

181 We now examine the effect of different surface restoring time scales on
 182 the response of the Southern Ocean to wind stress changes using an idealised
 183 Southern Ocean channel model setup similar to Abernathey et al. (2011).

184 The model used in this study is the MIT general circulation model (MIT-
 185 gcm; Marshall et al. (1997)). The model domain is a zonally re-entrant
 186 channel that is 1000 km in zonal extent, 2000 km in meridional extent, and
 187 2985 m deep with a flat bottom. There are 33 geopotential levels whose
 188 thickness increases with depth, ranging from 10 m at the surface to 250 m
 189 at the bottom. The horizontal grid spacing is chosen to be 10 km that is
 190 sufficiently fine to permit a vigorous eddy field but not so computational
 191 expensive that a large number of sensitivity experiments can be conducted.
 192 Additional model runs at a finer resolution (i.e., 5 km) reveal only small
 193 quantitative differences. The model uses a linear equation of state and has
 194 no salinity such that the model density depends only on temperature. We

²In this simple model, changes of Ψ^* tend to over-compensate for changes of $\bar{\Psi}$, which may be related to a number of simplifications invoked here such as uniform s and invariant \bar{B} . If changes in \bar{B} are taken into account, $\Delta\Psi_{res} \approx -\frac{\Delta\tau}{\rho_0 f} \left(\frac{\Psi_{res}}{2\Psi^*} \right) - \frac{1}{s} \frac{\Delta\bar{B}}{\partial b_N / \partial z}$, where $\Delta\bar{B}$ can be further related to changes in K and $\partial\bar{b}_s/\partial y$. Here we do not intend to provide a comprehensive quantitative solution to this problem, but simply use the qualitative arguments derived here to help interpret results obtained from our numerical experiments.

Table 1: Key physical and numerical parameters used in the model experiments.

| Symbol | Value | Description |
|-------------------------|---|------------------------------------|
| L_x, L_y | 1000 km, 2000 km | Domain size |
| H | 2985 m | Domain depth |
| $\Delta x, \Delta y$ | 10 km | Horizontal grid spacing |
| Δz | 10 to 250 m | Vertical grid spacing |
| τ_0 | 0, 0.1, 0.2, 0.3 N m ⁻² | Wind stress magnitude |
| Q_0 | 10 W m ⁻² | Surface heat flux magnitude |
| λ^{-1} | 1 day to infinity | Surface restoring time scale |
| λ_{sponge}^{-1} | 7 days | Sponge-layer relaxation time scale |
| r_b | 1.1×10^{-3} | Linear bottom drag coefficient |
| κ_v | 1×10^{-5} m ² s ⁻¹ | Vertical diffusivity |
| κ_h | 0 | Horizontal diffusivity |
| A_v | 1×10^{-3} m ² s ⁻¹ | Vertical viscosity |
| A_4 | 1×10^{10} m ⁴ s ⁻¹ | Horizontal biharmonic viscosity |

195 employ the K-profile parameterization (KPP) vertical mixing scheme (Large
 196 et al., 1994) and a linear bottom friction with drag coefficient of 1.1×10^{-3} .
 197 Table 1 lists the key physical and numerical parameters used in our model
 198 experiments.

199 The model is forced by zonal wind stress and heat fluxes at the surface
 200 and restored to a prescribed stratification profile, $T_N(z)$, in a sponge layer
 201 along the northern boundary on a short time scale of 7 days (Fig. 2). The
 202 surface heat flux and zonal wind stress take the same form as in Abernathey

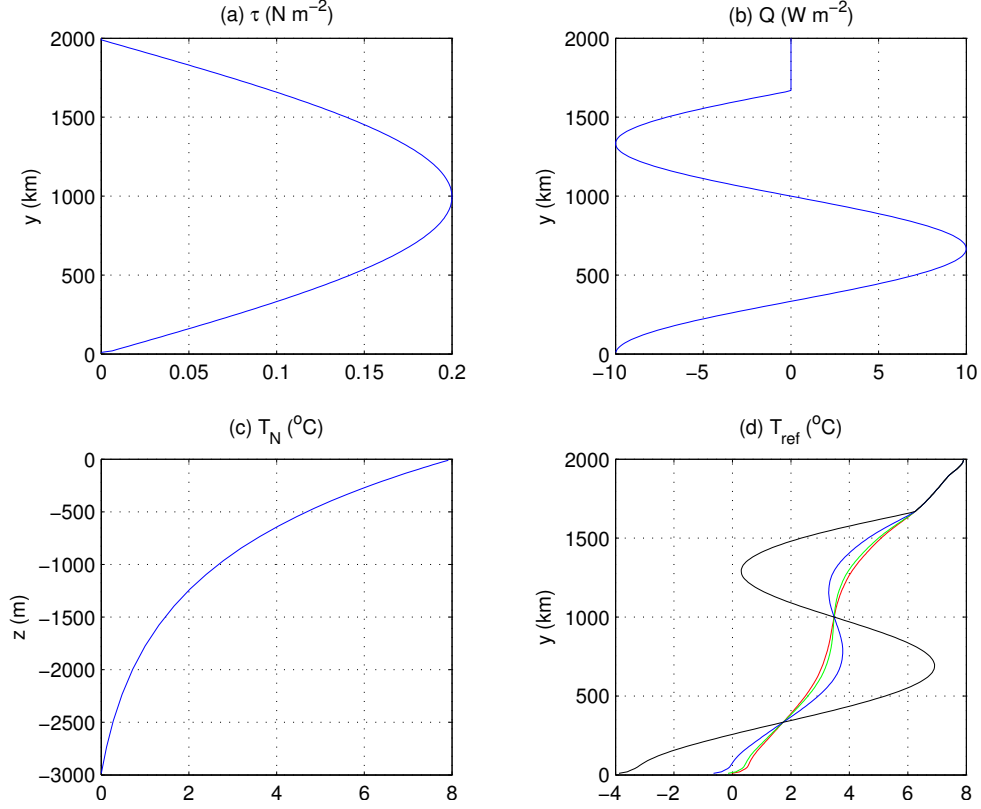


Figure 2: a) The surface wind stress τ , (b) surface heat flux Q , and (c) restoring temperature profile at the northern boundary used in the first 800-year spinup, and (d) the reference temperatures used for the second 300-year spinup. The red, green, blue and black lines in (d) are T_{ref} for model experiments with $\lambda^{-1} = 1$ day, 1 week, 1 month, and half a year, respectively.

et al. (2011):

$$Q(y) = \begin{cases} -Q_0 \cos(3\pi y/L_y) & \text{for } y < 5L_y/6 \\ 0 & \text{for } y > 5L_y/6 \end{cases} \quad (18)$$

and

$$\tau(y) = \tau_0 \sin(\pi y/L_y), \quad (19)$$

where $L_y = 2000$ km is the meridional width of the domain. During the first stage of model spinup, $Q_0 = 10 \text{ W m}^{-2}$ and $\tau_0 = 0.2 \text{ N m}^{-2}$. Readers are referred to Abernathey et al. (2011) for detailed motivation from observations for choosing the above forcing profiles. The purpose of the present study is to investigate the effect of different surface restoring time scales on the response of the Southern Ocean to wind stress changes, taking into account the qualitative arguments presented in Section 2.

The model was first spun up from rest with the above constant wind stress and heat flux forcing for 800 years to achieve a statistically steady state. After that, the model was run for another 300 years under the same wind stress forcing but with purely restoring surface heat flux forcing: the model surface temperature (T_s) is restored to reference temperatures (T_{ref}) at time scales of one day, one week, one month and half a year, respectively. The reference temperatures are determined in such a way that models with different restoring time scales have the same effective surface heat flux as the first 800-year spinup simulation, i.e.,

$$T_{ref} = T_s + \frac{Q}{\rho_0 c_p \lambda \Delta z}, \quad (20)$$

where $\Delta z = 10$ m is the thickness of the top model grid box, c_p is specific heat at constant pressure, and λ^{-1} is the restoring time scale. Here T_s is taken to

Table 2: Changes of surface eddy kinetic energy (ΔEKE in $\text{m}^2 \text{s}^{-2}$) in response to wind stress changes in model experiments with different surface restoring time scales. Note that $\lambda^{-1} = \text{infinity}$ corresponds to a fixed surface heat flux. The percentage change is relative to EKE at $\tau_0 = 0.2 \text{ N m}^{-2}$.

| λ^{-1} | $\tau_0 = 0 \text{ N m}^{-2}$ $\Delta\text{EKE} (\%)$ | $\tau_0 = 0.1 \text{ N m}^{-2}$ $\Delta\text{EKE} (\%)$ | $\tau_0 = 0.2 \text{ N m}^{-2}$ EKE | $\tau_0 = 0.3 \text{ N m}^{-2}$ $\Delta\text{EKE} (\%)$ |
|----------------|--|--|--|--|
| 1 day | -0.0046 (-16%) | -0.0024 (-8.6%) | 0.0280 | 0.0034 (12%) |
| 1 week | | -0.0053 (-18%) | 0.0297 | 0.0047 (16%) |
| 1 month | | -0.0072 (-23%) | 0.0315 | 0.0065 (21%) |
| half a year | | -0.0098 (-30%) | 0.0327 | 0.0082 (25%) |
| infinity | -0.0279 (-85%) | -0.0114 (-35%) | 0.0330 | 0.0091 (28%) |

223 be the time-mean surface temperature averaged over the last 100 years of the
 224 first 800-year spinup. It is evident from (20) that the reference temperatures
 225 are different for model experiments with different surface restoring time scales
 226 (see Fig. 2d).

227 After this second stage of spinup, the models with different surface restor-
 228 ing time scales were run for another 300 years forced by wind stress of dif-
 229 ferent strengths, i.e., different τ_0 (see Table 2 for a list of model experiments
 230 conducted). Results averaged over the last 100 years are used for this study.

231 Following Abernathey et al. (2011) and Munday and Zhai (2013), the
 232 residual MOC, Ψ_{res} , is diagnosed by computing the time-mean streamfunc-
 233 tion of the zonally-integrated thickness-weighted flow using the following in-
 234 tegral,

$$\Psi_{res}(y, \theta) = \frac{1}{\Delta t} \int_{t_0}^{t_0 + \Delta t} \int_0^{L_x} \int_{\theta_0}^{\theta} (hv) d\theta dx dt, \quad (21)$$

235 where $h = \partial z / \partial \theta$ is the layer thickness in potential temperature (θ) coordi-

236 nate, L_x is the zonal width of the channel, t is time, and $\Delta t = 100$ years.
 237 The integral in Eq. (21) is calculated using discrete layers that are 0.2°C
 238 thick with potential temperature used as the vertical coordinate, which is
 239 then converted back to depth coordinates. Finally, the eddy-induced MOC
 240 is diagnosed as the residual: $\Psi^* = \Psi_{res} - \bar{\Psi} = \Psi_{res} + \tau/(\rho_0 f)$.

241 4. Results

242 4.1. Spinup

243 After the first 800-year spinup, the model reaches a statistically steady
 244 state and produces a vigorous eddy field, as demonstrated by the instan-
 245 taneous surface temperature at the end of the spinup. Both the pattern
 246 and magnitude of the residual MOC averaged over the last 100 years of the
 247 spinup are very similar to those from the fixed surface flux experiment in
 248 Abernathey et al. (2011). The residual MOC is characterised by three dis-
 249 tinct cells, and is, importantly, directed along the mean isotherms in the
 250 interior of the model domain (Fig. 3a), consistent with the assumption made
 251 in Section 2. These three overturning cells are closed by diabatic circula-
 252 tion in the surface diabatic and northern sponge layers. The branch of the
 253 broad upwelled water that travels north first gains buoyancy through surface
 254 heating but eventually encounters a region of surface cooling and subducts
 255 along the 4°C isotherm, forming the clockwise upper cell with a strength of
 256 ~ 0.6 Sv. The branch of the upwelled water that travels south quickly loses
 257 buoyancy due to surface heat loss and subducts along the 0.5°C isotherm, re-
 258 sulting in the coldest water in the domain and forming the counterclockwise
 259 deep cell with a strength of ~ 0.2 Sv.

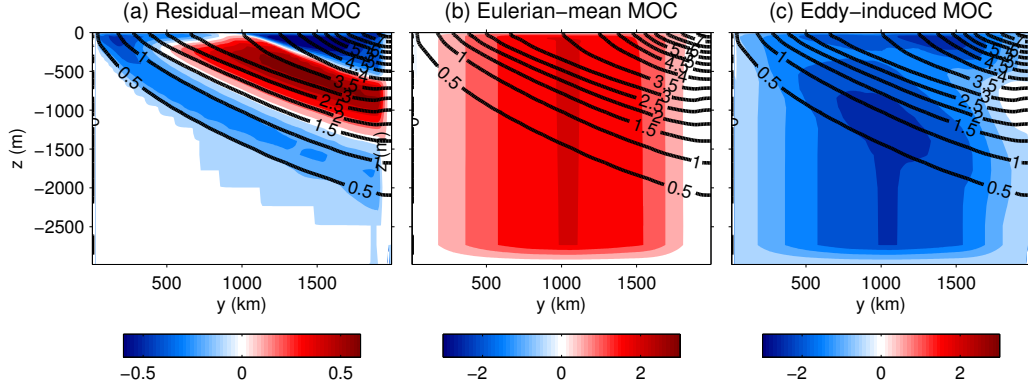


Figure 3: (a) The residual-mean, (b) Eulerian-mean and (c) eddy-induced MOCs averaged over the last 100 years of the first 800-year spinup model run in Sv. The black contours are the mean isotherms and the contour interval of the MOCs is 0.1 Sv in (a) but 0.5 Sv in (b) and (c).

260 These two overturning cells loosely resemble the gross circulation features
 261 observed in the Southern Ocean: upwelling of the North Atlantic Deep Water
 262 and subduction of the Antarctic Intermediate Water and Bottom Water (e.g.
 263 Rintoul et al., 2001), although it is worth emphasising the idealised nature of
 264 the model configuration. For example, bottom topography, which is known
 265 to play an important role in the formation of the deep cell in the Southern
 266 Ocean, is absent in this model. To the north of the upper cell, there is
 267 another counterclockwise overturning cell, but this cell is very shallow and
 268 contained mostly in the surface and northern diabatic layers. In this study,
 269 unless stated otherwise, we will focus primarily on the upper cell and its
 270 response to changes of wind stress. Figure 3 shows that the residual MOC
 271 results from cancellation of the much stronger Eulerian-mean MOC and eddy-
 272 induced MOC (see Eq. (2)). So far the first 800-year spinup has successfully
 273 reproduced the control experiment in Abernathey et al. (2011), albeit that

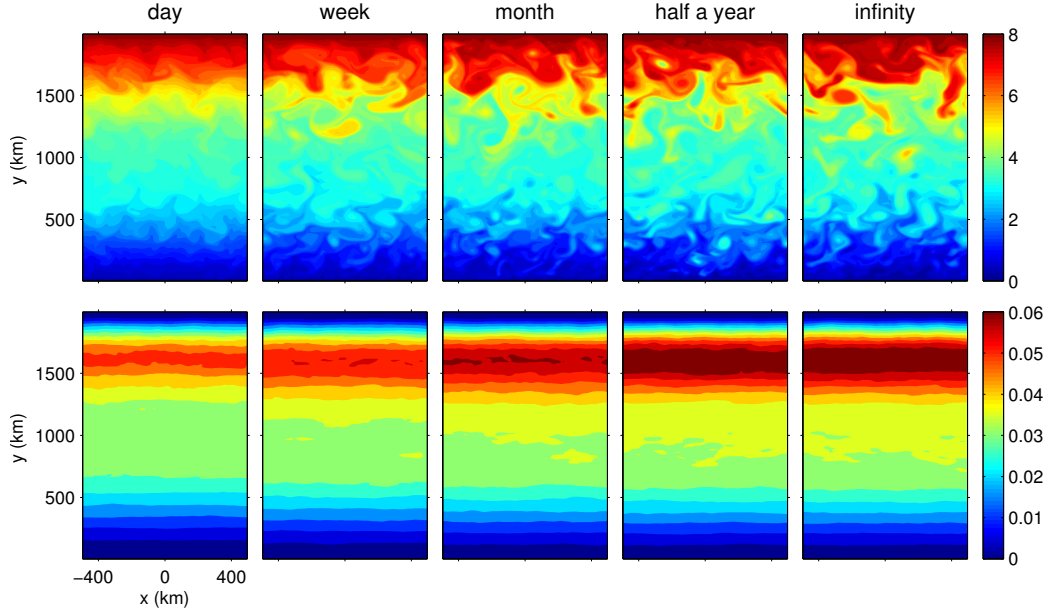


Figure 4: (The top row) The instantaneous surface temperature ($^{\circ}\text{C}$) at the end of the 300-year spinup with $\lambda^{-1} = 1$ day, 1 week, 1 month, half a year and infinity, respectively, and (the bottom row) surface EKE ($\text{m}^2 \text{s}^{-2}$) averaged over the last 100 years of this second stage of spinup.

the deep cell in our model is slightly weaker.

Over the next 300 years, the model is subject to the same wind stress forcing with $\tau_0 = 0.2 \text{ N m}^{-2}$ but surface heat fluxes that result from restoring boundary conditions at various restoring time scales, λ^{-1} , ranging from one day to infinity (i.e., a fixed surface heat flux). Figure 4 shows the instantaneous surface temperature fields at the end of year 300 and surface EKE averaged over the last 100 years in model experiments with various λ^{-1} . As λ^{-1} decreases from infinity to one day, surface temperature variability is increasingly damped owing to the increasingly efficient air-sea damping of surface eddy temperature variance (e.g. Zhai and Greatbatch, 2006b; Great-

batch et al., 2007; Shuckburgh et al., 2011), although the time-mean surface temperature remains almost identical across all these experiments. The magnitude of surface EKE decreases everywhere with decreasing restoring time scale such that the surface EKE in the experiment with $\lambda^{-1} = 1$ day is on average about 15% weaker than that in the experiment with $\lambda^{-1} = \text{half a year}$. However, the influence of different surface restoring time scales on EKE decays rapidly with depth and becomes almost undetectable below the top 150 m (Fig. 5a). In contrast, the influence of air-sea damping on temperature variance extends at least twice as deep (Fig. 5b).

The net surface restoring heat fluxes in all these model experiments are similar to the constant surface heat flux used in the first 800-year spinup, although there are some differences when the restoring time scale becomes very short (not shown). Figure 6 shows the residual MOCs in experiments with different λ^{-1} . Apart from the differences in the surface diabatic layer, the residual MOCs in all the restoring model runs are comparable to each other, as well as to that in the first 800-year spinup (Fig. 3a).

4.2. *Response to wind stress changes*

After all the restoring model runs reach statistically steady states, we increase and decrease τ_0 by 0.1 N m^{-2} and let the model run for another 300 years to reach a new equilibria. Figure 7 shows the changes of the residual MOCs averaged over the last 100 years when τ_0 increases from 0.2 to 0.3 N m^{-2} . The increased wind stress is found to create anomalous clockwise overturning cells below the surface diabatic layer in all the restoring experiments. The strength and extent of these anomalous cells, however, varies with the restoring time scale, with greater changes seen for shorter restor-

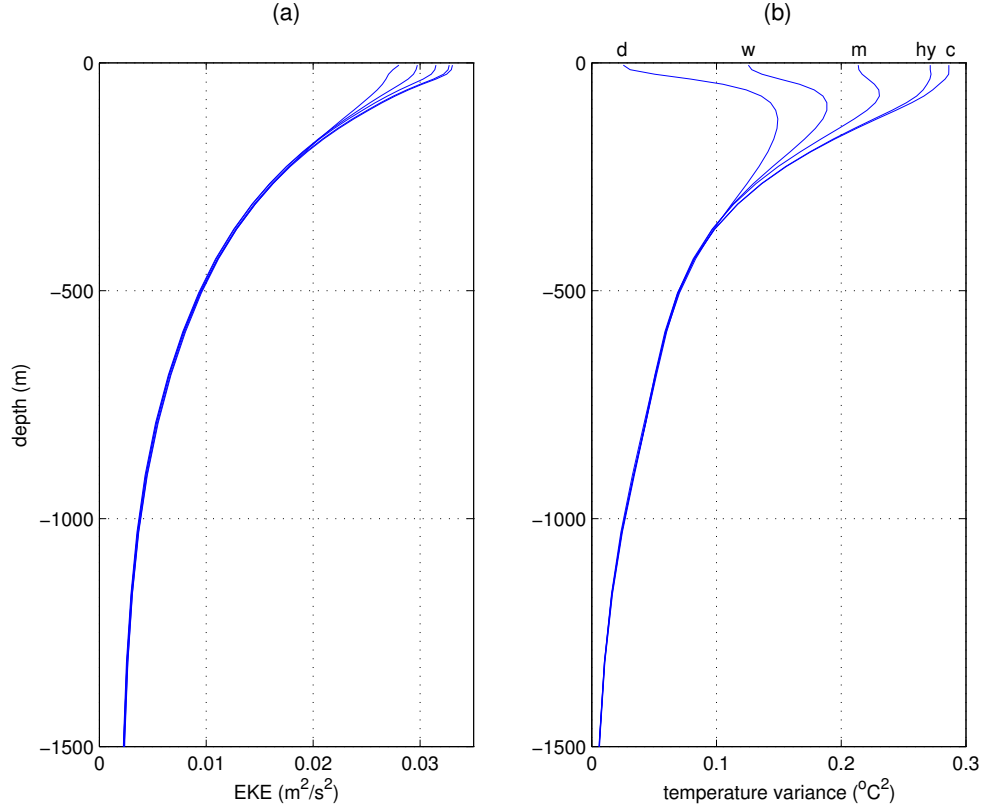


Figure 5: Horizontally-averaged (a) EKE ($\text{m}^2 \text{s}^{-2}$) and (b) temperature variance ($^\circ\text{C}^2$) in the 300-year spinup model runs with various surface restoring time scales. Letters “d”, “w”, “m”, “hy” and “c” denote model experiments with $\lambda^{-1} = 1$ day, 1 week, 1 month, half a year, and infinity, respectively. The curves in (a) are in the same order as those in (b), but are not labelled for the sake of clarity.

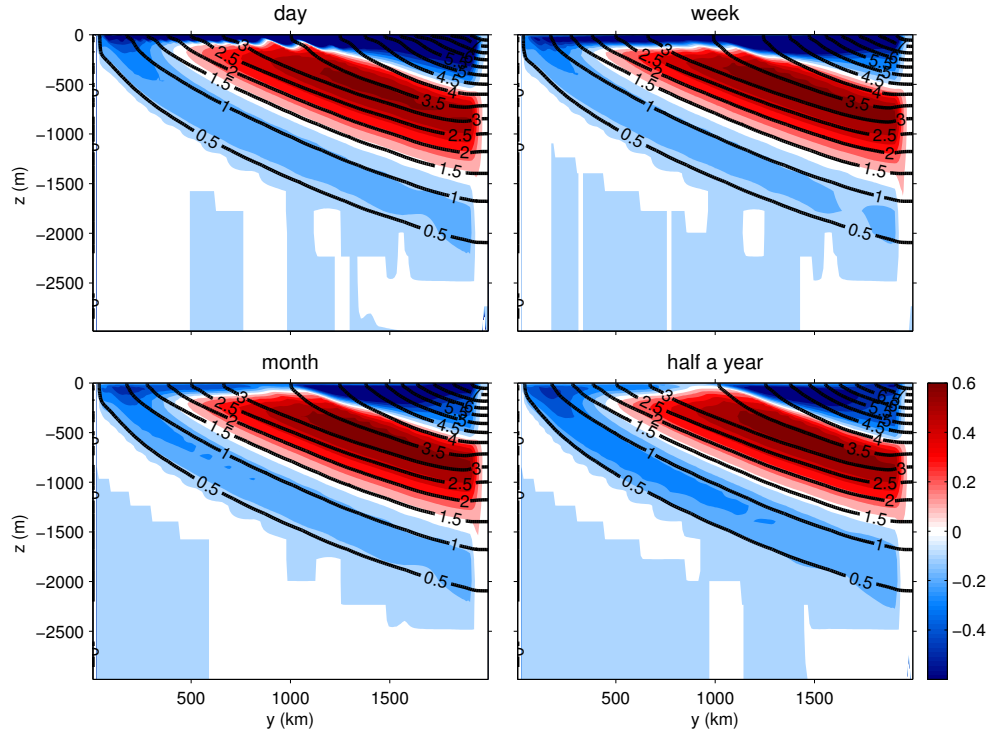


Figure 6: The residual MOCs (Sv) in the 300-year spinup model runs with $\lambda^{-1} = 1$ day, 1 week, 1 month, and half a year, respectively. The black contours are the mean isotherms in each experiment and the contour interval of the MOCs is 0.1 Sv.

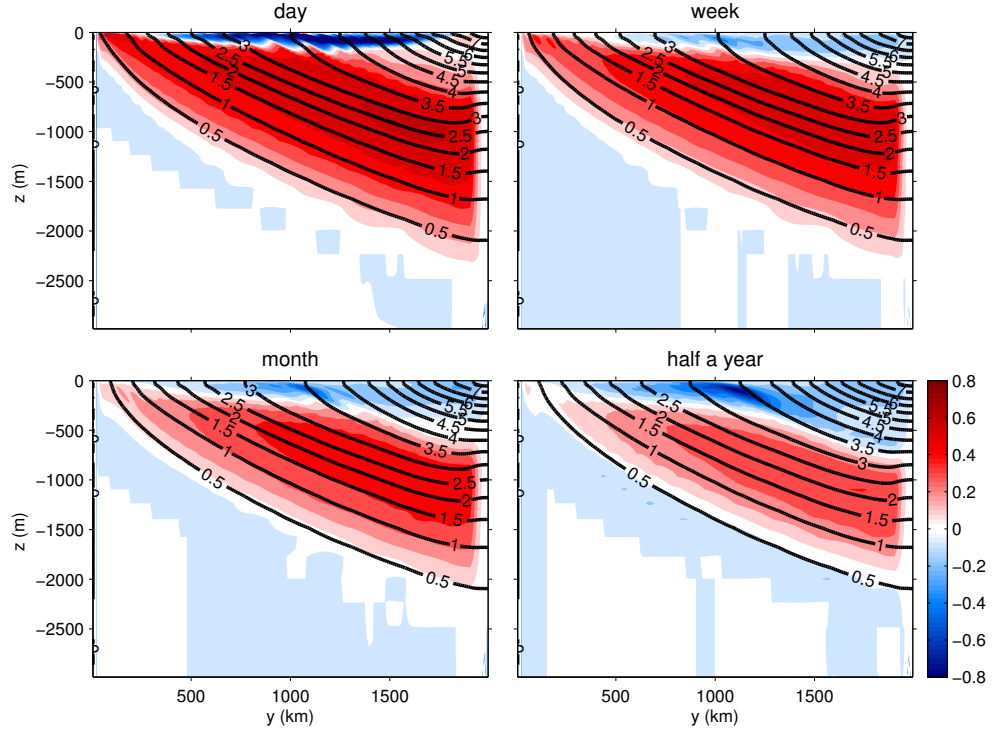


Figure 7: Changes of the residual MOCs (Sv) when the wind stress increases from 0.2 to 0.3 N m^{-2} in experiments with $\lambda^{-1} = 1 \text{ day}$, 1 week , 1 month , and half a year , respectively. The black contours are the mean isotherms in each experiment when $\tau_0 = 0.3 \text{ N m}^{-2}$ and the contour interval of the MOCs is 0.1 Sv .

309 ing time scales. For example, the maximum changes associated with these
 310 anomalous cells in experiments with $\lambda^{-1} = 1$ day, 1 week, 1 month and half
 311 a year are 0.69 Sv, 0.57 Sv, 0.48 Sv, 0.40 Sv, respectively. Since the change
 312 in the Eulerian-mean MOCs ($\Delta\bar{\Psi} \simeq 1$ Sv) due to increased wind stress is
 313 identical across all the model experiments, differences in the response of the
 314 residual MOCs must be entirely due to differences in the response of the
 315 eddy-induced MOCs (Fig. 8).

316 The overall patterns of the response of the eddy-induced MOCs are very
 317 similar among experiments with different restoring time scales: Ψ^* increases
 318 in strength in response to the increase in wind stress almost everywhere in
 319 the model domain. However, the magnitude of this increase in Ψ^* is sensitive
 320 to the surface restoring time scale: longer λ^{-1} results in a larger increase in
 321 Ψ^* . The magnitude of Ψ^* is found to increase, on average, by about 0.2
 322 Sv more, when $\lambda^{-1} =$ half a year than when $\lambda^{-1} = 1$ day (Fig. 8d minus
 323 Fig. 8a), excluding the top few tens of meters. Changes of the residual and
 324 eddy-induced MOCs when the wind stress weakens from 0.2 to 0.1 N m^{-2}
 325 generally mirror those when the wind stress strengthens from 0.2 to 0.3 N
 326 m^{-2} (not shown): larger decrease in the strength of Ψ^* and thus smaller
 327 decrease of Ψ_{res} at longer restoring time scales. The maximum changes of
 328 the residual MOCs in experiments with $\lambda^{-1} = 1$ day, 1 week, 1 month and
 329 half a year are -0.69 Sv, -0.59 Sv, -0.52 Sv, -0.45 Sv, respectively.

330 The response of the residual and eddy-induced MOCs to changes in wind
 331 stress as well as differences among experiments with different λ^{-1} is broadly
 332 consistent with arguments presented in Section 2 for the strong and weak
 333 surface restoring limits. In the strong restoring limit, e.g., $\lambda^{-1} = 1$ day,

Table 3: Strength of the residual MOC of the upper cell (in Sv) below the surface diabatic layer in model experiments with different surface restoring time scales and wind forcing.

| λ^{-1} | $\tau_0 = 0.1 \text{ N m}^{-2}$ | $\tau_0 = 0.2 \text{ N m}^{-2}$ | $\tau_0 = 0.3 \text{ N m}^{-2}$ |
|----------------|---------------------------------|---------------------------------|---------------------------------|
| 1 day | 0.05 | 0.63 | 1.20 |
| 1 week | 0.12 | 0.65 | 1.17 |
| 1 month | 0.21 | 0.65 | 1.04 |
| half a year | 0.36 | 0.64 | 0.88 |
| infinity | 0.52 | 0.64 | 0.82 |

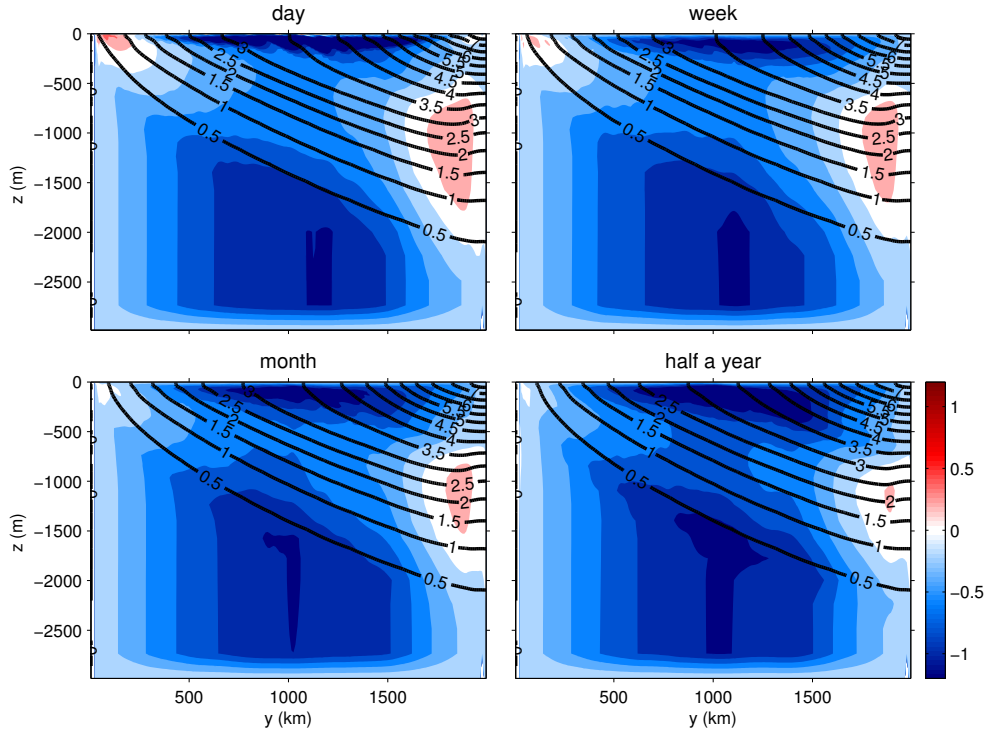


Figure 8: Changes of the eddy-induced MOCs (Sv) when the wind stress increases from 0.2 to 0.3 N m⁻² in experiments with $\lambda^{-1} = 1$ day, 1 week, 1 month, and half a year, respectively. The black contours are the mean isotherms in each experiment when $\tau_0 = 0.3$ N m⁻² and the contour interval of the MOCs is 0.2 Sv.

334 temperature at the surface, as well as at the northern boundary, is effec-
 335 tively prescribed, leaving the isothermal slopes little freedom to vary (Fig.
 336 9a). Since the eddy-induced MOC is, to a large extent, determined by the
 337 isothermal slopes according to the scaling argument in Section 2, changes of
 338 the eddy-induced MOC, and therefore the ability of eddies to compensate
 339 for changes of wind stress, are strongly suppressed. As a result, the residual
 340 MOC exhibits a greater sensitivity to wind stress changes when $\lambda^{-1} = 1$ day.

341 As the restoring time scale lengthens, the isotherms at the surface become
 342 less constrained by the restoring and more able to move in response to wind
 343 stress changes (Figs. 9b-d). The isothermal slopes are thus increasingly
 344 free to steepen when the wind stress strengthens or slump when the wind
 345 stress weakens. This leads to a strengthening or weakening of the eddy
 346 field, which acts to compensate for wind stress changes. As a consequence,
 347 the residual MOC exhibits a much weaker sensitivity to wind stress changes
 348 when $\lambda^{-1} = \text{half a year}$. The reduced sensitivity of the residual MOC at
 349 longer λ^{-1} is consistent with the smaller changes of surface heat fluxes in
 350 experiments with longer λ^{-1} (Fig. 10). Note that changes in surface heat
 351 fluxes in our experiments are results of the response of the Southern Ocean
 352 MOC to changes in wind stress such that in thermodynamic equilibrium the
 353 residual MOC matches the diabatic forcing (e.g. Walin, 1982; Watson and
 354 Naveira Garabato, 2006; Badin and Williams, 2010). Readers are referred to
 355 Morrison et al. (2011) for an example of the response of the Southern Ocean
 356 MOC to imposed changes in buoyancy forcing in the absence of wind stress
 357 changes.

358 Figure 11 shows changes of the horizontally-averaged EKE in experiments

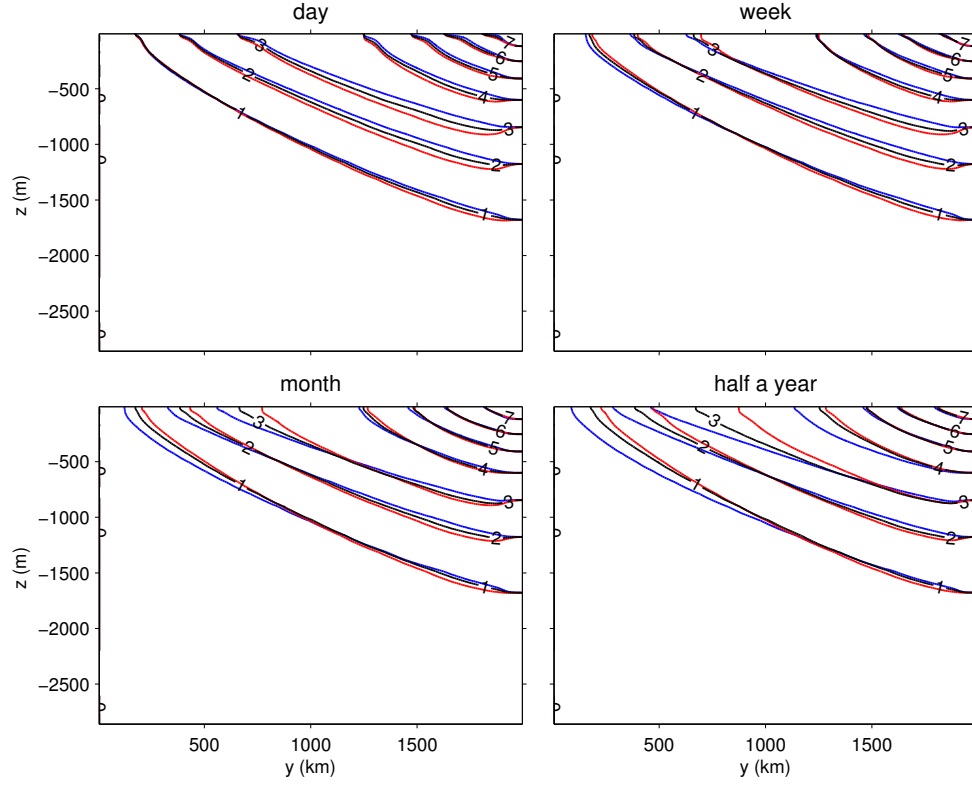


Figure 9: The time- and zonal-mean temperatures ($^{\circ}\text{C}$) in experiments with $\lambda^{-1} = 1$ day, 1 week, 1 month, and half a year for $\tau_0 = 0.1 \text{ N m}^{-2}$ (blue curve), 0.2 N m^{-2} (black curve), and 0.3 N m^{-2} (red curve).

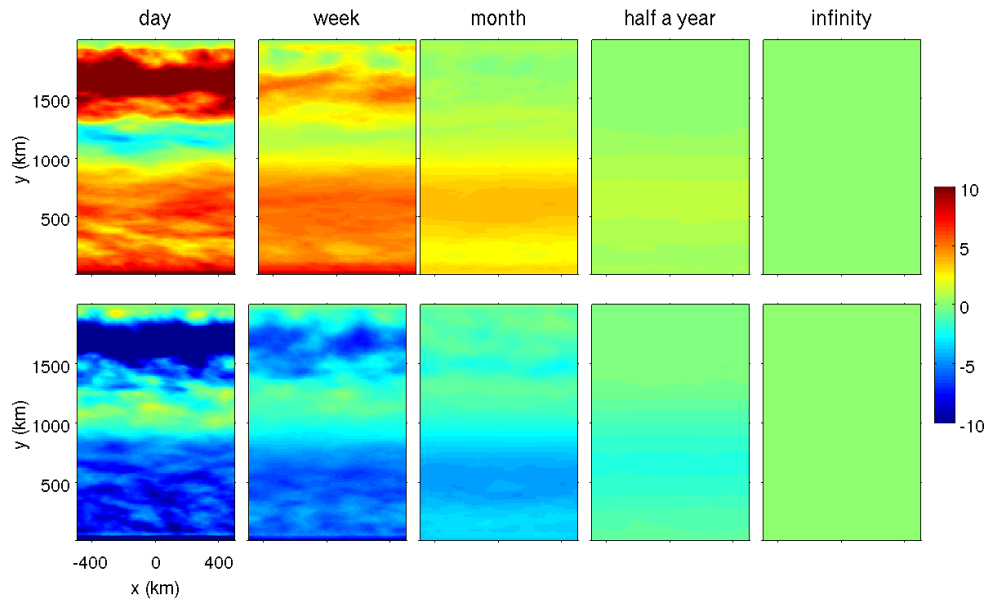


Figure 10: Changes of the net surface heat fluxes (W m^{-2}) in experiments with $\lambda^{-1} = 1$ day, 1 week, 1 month, half a year and infinity, when τ_0 increases from 0.2 to 0.3 N m^{-2} (top row) and decreases from 0.2 to 0.1 N m^{-2} (bottom row). Positive values mean the ocean gains more heat.

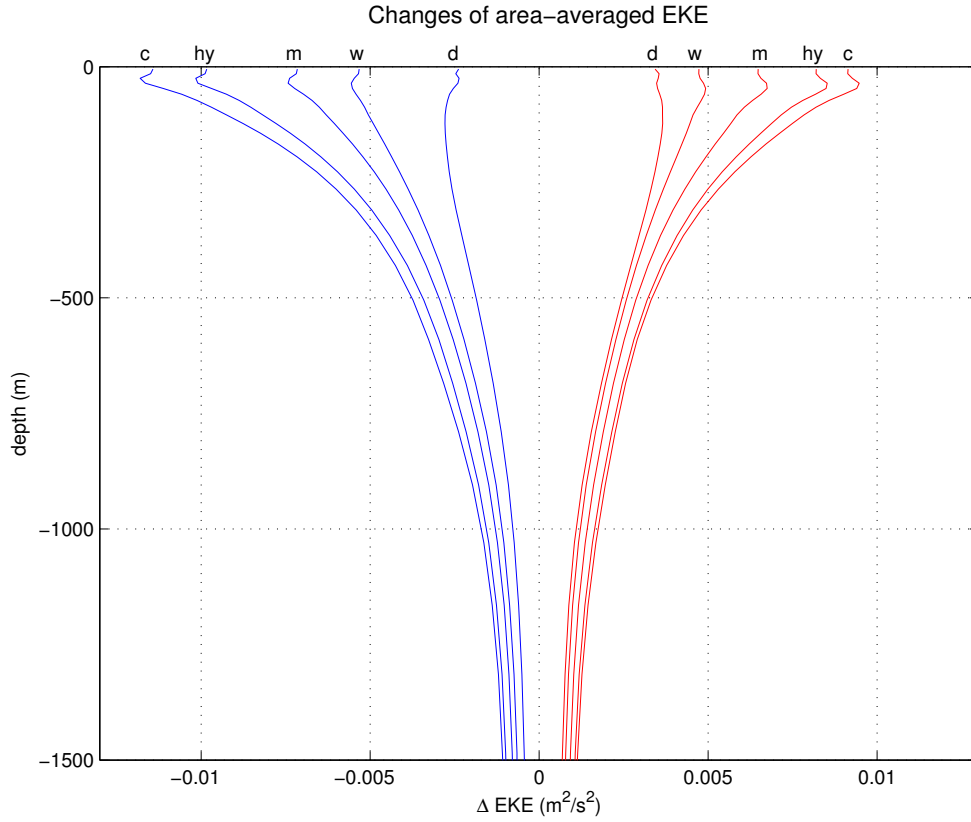


Figure 11: Changes of the horizontally-averaged EKE ($\text{m}^2 \text{s}^{-2}$) when the wind stress increases from 0.2 to 0.3 N m^{-2} (red curves) and decreases from 0.2 to 0.1 N m^{-2} (blue curves). Letters “d”, “w”, “m”, “hf” and “c” denote model experiments with $\lambda^{-1} = 1$ day, 1 week, 1 month, half a year, and infinity, respectively.

359 with different λ^{-1} , which clearly demonstrates the sensitivity of the eddy
 360 response to the surface restoring time scale. As the restoring time scale
 361 increases, EKE in our model becomes increasingly sensitive to wind stress
 362 changes. For example, in response to the strengthening of wind stress from
 363 0.2 to 0.3 N m⁻², EKE at the surface increases by 12%, 16%, 21%, 25%
 364 and 28% in experiments with $\lambda^{-1} = 1$ day, 1 week, 1 month, half a year and
 365 infinity, respectively (see Table 2). A slightly greater change is seen when the
 366 wind stress relaxes from 0.2 to 0.1 N m⁻², where the surface EKE is found to
 367 decrease by 8.6%, 18%, 23%, 30% and 35% in experiments with $\lambda^{-1} = 1$ day,
 368 1 week, 1 month, half a year and infinity, respectively. Note that changes of
 369 the EKE in response to wind stress changes are not confined in the upper
 370 ocean but extends all the way to the bottom, and so does the influence of
 371 different restoring time scales on such changes.

372 Adopting a simple flux gradient closure for the eddy buoyancy flux, the
 373 eddy diffusivity, $K(y, z)$, can be diagnosed using

$$K(y, z) = -\frac{\overline{v'T'}}{\overline{T}_y}, \quad (22)$$

374 where $v'T'$ is the meridional eddy heat flux, T_y is the meridional temperature
 375 gradient, overbars denote a 100-year average and primes are deviations from
 376 it. Figure 12 shows the zonally-averaged K for different values of τ_0 at
 377 $\lambda^{-1} = 1$ day and $\lambda^{-1} = \text{infinity}$, respectively. Similar to Abernathey et al.
 378 (2011), K is found to be intensified near the very surface and toward the
 379 bottom, with a minimum at mid-depth. The magnitude of K increases with
 380 increasing wind stress for all λ^{-1} , but the spatial pattern of K does not
 381 appear to be sensitive to either τ_0 or λ^{-1} . The degree of changes in K in
 382 response to changes in wind stress, however, depends on λ^{-1} , with greater

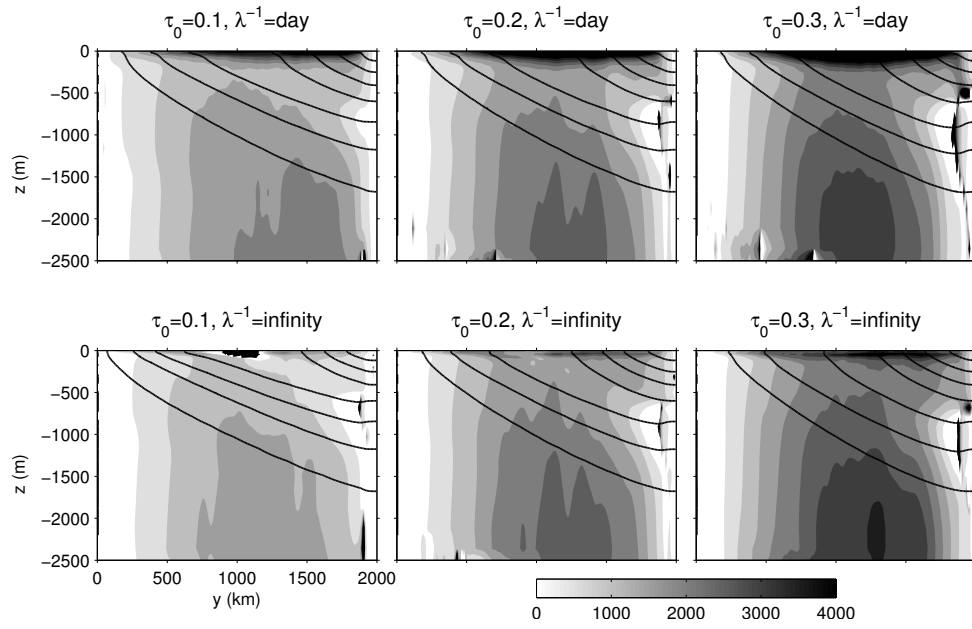


Figure 12: Zonally-averaged eddy thickness diffusivity $K(y, z)$ with contour interval of $500 \text{ m}^2 \text{ s}^{-1}$ in experiments with $\lambda^{-1} = 1 \text{ day}$ (top row) and $\lambda^{-1} = \text{infinity}$ (bottom row), respectively. The black contours are the mean isotherms in each experiment, and the contour interval is 1°C .

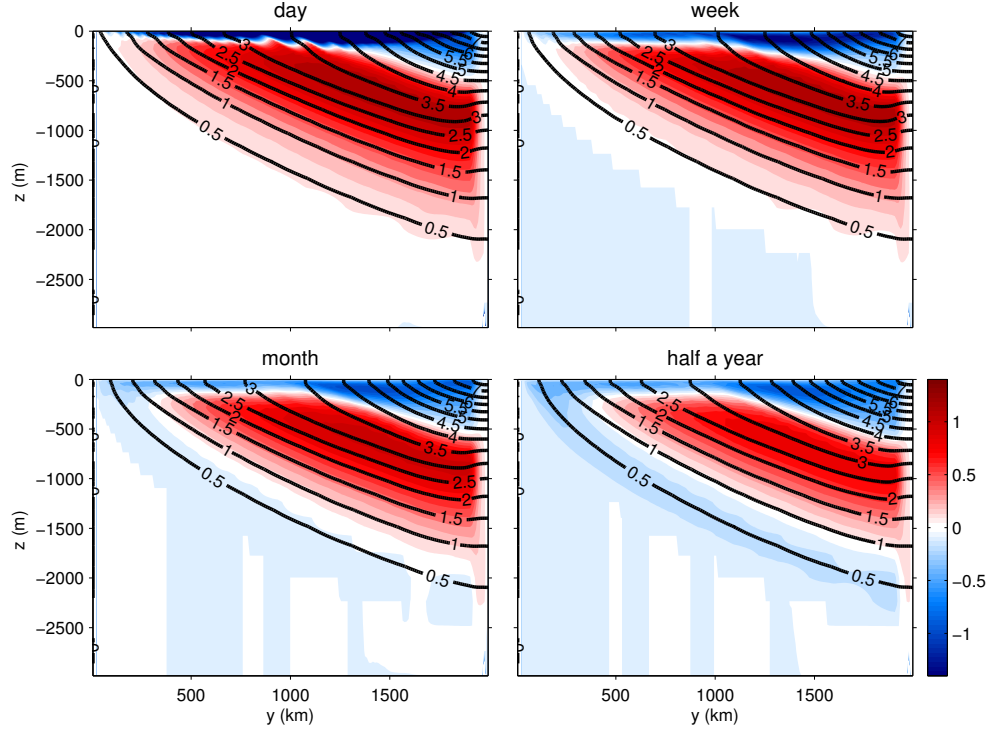


Figure 13: The residual MOCs (Sv) when $\tau_0 = 0.3 \text{ N m}^{-2}$ in experiments with $\lambda^{-1} = 1 \text{ day}$, 1 week, 1 month, and half a year, respectively. The black contours are the mean isotherms in each experiment and the contour interval of the MOCs is 0.1 Sv.

changes found at longer λ^{-1} . For example, when τ_0 decreases from 0.2 to 0.1 N m^{-2} , K decreases on average by about $600 \text{ m}^2 \text{ s}^{-1}$ in experiment with $\lambda^{-1} = 1 \text{ day}$, but by more than $900 \text{ m}^2 \text{ s}^{-1}$ in experiment with $\lambda^{-1} = \text{infinity}$. The greater sensitivity of K to wind stress changes at longer λ^{-1} is consistent with the greater sensitivities of isothermal slopes and EKE at longer λ^{-1} as well as the scaling arguments presented in Section 2.

We now come back to interpret the residual MOCs in experiments with different λ^{-1} when the wind stress strengthens (Fig. 13). At $\lambda^{-1} = 1 \text{ day}$,

391 the lower cell disappears and the upper cell becomes significantly stronger,
 392 resulting in an overall clockwise cell below the surface diabatic layer. With
 393 the wind stress increasing to 0.3 N m^{-2} , the strength of the Eulerian-mean
 394 MOC increases by 1 Sv, that is, a 50% increase. On the other hand, the
 395 vigour of eddy activity is maintained by the sloping isotherms that are held
 396 more or less constant by strong restoring at the surface as well as at the
 397 northern boundary, regardless of the increase in wind stress. Table 2 shows
 398 that the surface EKE increases by only 12%, and is thus unable to keep up
 399 with wind stress changes. In the case of an increase in wind stress, restoring
 400 at the surface acts as an extra energy sink for the system by preventing the
 401 isotherms from tilting further. As a result, the strength of the residual MOC
 402 below the surface diabatic layer becomes almost doubled, increasing by 0.57
 403 Sv (see Table 3). Note that this is less than the maximum increase of 0.69
 404 Sv found in Fig. 7a because the maximum increase of the residual MOC
 405 (Fig. 7a) and the maximum residual MOC itself (Fig. 6a) do not overlap in
 406 space. Apparently even at $\lambda^{-1} = 1$ day there is still some eddy compensation
 407 effect, and as such the increase of the residual MOC is still less than the 1
 408 Sv increase of the Eulerian-mean MOC. At $\lambda^{-1} = \text{half a year}$, when the
 409 wind stress increases to 0.3 N m^{-2} , the isothermal slopes become steeper,
 410 which leads to an enhanced eddy activity that is able to compensate for the
 411 majority of the increase in the Eulerian-mean MOC. For example, the surface
 412 EKE increases by about 25% (Table 2), more than double of the percentage
 413 increase when $\lambda^{-1} = 1$ day. As a result, the strength of the residual MOC
 414 below the surface diabatic layer increases only by about 0.24 Sv (Table 3),
 415 less than half of the increase when $\lambda^{-1} = 1$ day. Furthermore, the pattern of

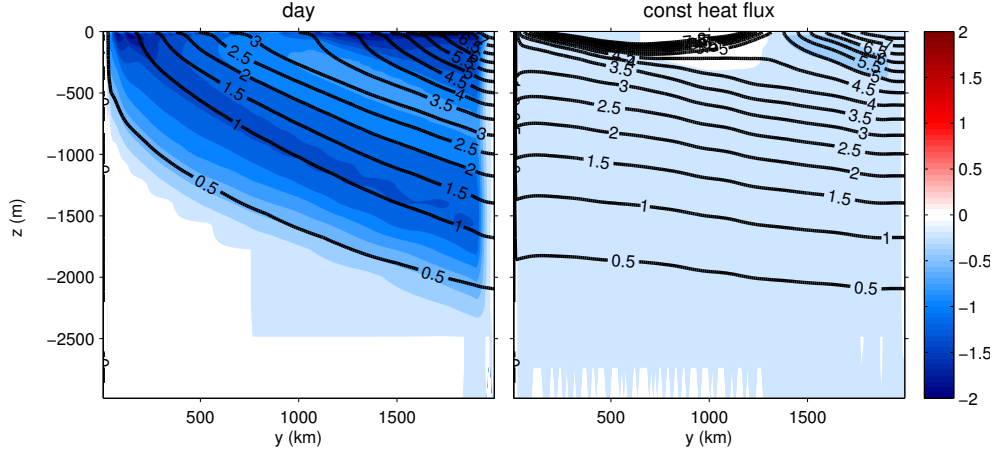


Figure 14: The residual MOCs (Sv) when the wind stress vanishes in experiments with $\lambda^{-1} = 1$ day and $\lambda^{-1} = \text{infinity}$. The black contours are the mean isotherms in each experiment and the contour interval of the MOCs is 0.2 Sv.

the residual MOC in the case of $\lambda^{-1} = \text{half a year}$ (Fig. 13d) resembles that when $\tau_0 = 0.2 \text{ N m}^{-2}$ (Fig. 6d).

Two additional model experiments were conducted with zero wind stress and at two restoring limits, i.e., $\lambda^{-1} = 1$ day and $\lambda^{-1} = \text{infinity}$, respectively (Fig. 14). Since the Eulerian-mean MOC vanishes with zero wind stress, the residual MOC is driven entirely by eddies. In the experiment where $\lambda^{-1} = 1$ day, the residual MOC is characterised by an overall counterclockwise circulation above the 0.5°C isotherm. Note that the eddy-induced MOC with vanishing wind stress is now directed along the mean isotherms in the interior of the model domain, in contrast to the situation where the wind stress is finite (Fig. 3c). Strong restoring at the surface is clearly capable of maintaining a vigorous residual MOC by supplying mean APE to the system and acting as an energy source for eddies. At $\lambda^{-1} = 1$ day, the surface EKE in

429 the experiment with vanishing wind stress is only 16% weaker than that in
 430 the experiment where $\tau_0 = 0.2 \text{ N m}^{-2}$ (Table 2). In contrast, in the experi-
 431 ment with a fixed surface heat flux, i.e., $\lambda^{-1} = \text{infinity}$, the isotherms become
 432 almost flat below the surface diabatic layer. There is only a weak residual
 433 MOC associated with a weak eddy field generated by constant surface heat-
 434 ing and cooling (e.g. Munday and Zhai, 2013). With a fixed surface heat
 435 flux, the surface EKE in the experiment with vanishing wind stress is about
 436 85% less than that in the experiment where $\tau_0 = 0.2 \text{ N m}^{-2}$ (Table 2).

437 **5. Summary and Discussion**

438 In this study, we have investigated the influence of different surface restor-
 439 ing times scales on the response of the Southern Ocean overturning to changes
 440 of the wind forcing, extending the recent work by Abernathey et al. (2011).
 441 Results from our idealised eddy-permitting model experiments broadly agree
 442 with the simple arguments derived from the residual-mean framework of Mar-
 443 shall and Radko (2003). Regardless of the restoring time scale chosen, the
 444 eddy-induced MOC is found to compensate for changes of the direct wind-
 445 driven Eulerian-mean MOC, rendering the residual MOC less sensitive than
 446 the Eulerian-mean MOC to wind stress changes. Our results thus add sup-
 447 port to the concept of eddy compensation (Viebahn and Eden, 2010). How-
 448 ever, the extent of this compensation depends strongly on the surface restor-
 449 ing time scale: residual MOC sensitivity increases with decreasing restoring
 450 time scale. Since changes of the Eulerian-mean MOCs are almost identical in
 451 experiments with different restoring time scales, the different degrees of com-
 452 pensation are due entirely to differences in the response of the eddy-induced

453 MOCs to wind stress changes.

454 The picture that emerges from our model study is as follows. The in-
455 crease in wind stress enhances the Eulerian-mean MOC that acts to further
456 steepen the tilted isopycnals and increase the mean APE of the system. In
457 the case of weak surface restoring, the isopycnals at the surface are free to
458 move around and as such the isopycnal surfaces steepen, which leads to the
459 generation of a more vigorous eddy field. The associated enhanced eddy-
460 induced MOC opposes the increase in the Eulerian-mean MOC, resulting
461 in smaller changes in the residual MOC. In contrast, in the case of strong
462 surface restoring, the isopycnals at the surface are pinned there, unable to
463 move around in response to wind stress changes, and the isopycnal surfaces
464 consequently do not steepen. The action of wind stress to increase the mean
465 APE is directly counterbalanced by surface restoring, leaving the eddy field
466 largely unchanged. As a result, the eddy-induced MOC is unable to keep up
467 with the increase in the Eulerian-mean MOC, leading to a higher degree of
468 sensitivity of the residual MOC. The impact of surface restoring is particu-
469 larly striking in experiments with vanishing wind stress, where restoring at a
470 short time scale is found to be capable of maintaining an eddy-induced MOC
471 of considerable strength by supplying mean APE to the system.

472 In addition to the eddy compensation effect on the MOC, recent eddy-
473 resolving and eddy-permitting model studies (e.g. Hallberg and Gnanade-
474 sikan, 2006; Farneti et al., 2010; Munday et al., 2013) show that the presence
475 of eddies also significantly limits the sensitivity of the Antarctic Circumpolar
476 Current (ACC) volume transport in response to changes in wind stress. For
477 example, the ACC transport increases by only about 10% to 20% in most

478 eddy-permitting models when the Southern Ocean wind stress is doubled.
479 This phenomenon is termed *eddy saturation* (Straub, 1993).

480 Eddy saturation and eddy compensation are often believed to be dynam-
481 ically linked: changes of the eddy-induced MOC compensate for changes of
482 the direct wind-driven MOC, reduces the increase in the tilt of the isopycnals,
483 and thereby limits the sensitivity of the (baroclinic) ACC transport through
484 thermal wind relation. The implication is that if the ACC transport is eddy
485 saturated, the Southern Ocean MOC is also eddy compensated. However, in
486 a recent idealised model study at both eddy-permitting and eddy-resolving
487 resolutions, Morrison and Hogg (2013) found significant differences between
488 the sensitivities and the resolution dependence of the Southern Ocean MOC
489 and the ACC transport in response to wind stress changes and they suggested
490 that eddy saturation and eddy compensation are controlled by distinct dy-
491 namical mechanisms.

492 Results from our simple model corroborate the findings of Morrison and
493 Hogg (2013): there is no one-to-one relationship between eddy saturation
494 and eddy compensation. At the shorter surface restoring time scale, the
495 (baroclinic) ACC transport in our model is insensitive (or saturated) to wind
496 stress changes owing to the largely prescribed isopycnal slopes, whereas the
497 RMOC varies considerably and is clearly less eddy compensated. At the
498 longer restoring time scale, the (baroclinic) ACC transport becomes more
499 variable, i.e., less saturated, owing to changes of the isopycnal slopes, while
500 the RMOC becomes much more eddy-compensated. Interestingly, our simple
501 model suggests that the degrees of eddy saturation and eddy compensation
502 vary in the opposite sense as a function of the surface restoring time scale.

503 This distinction between eddy saturation and eddy compensation bears
 504 significance for interpreting past and future observations. For example,
 505 Böning et al. (2008) analysed the Argo network of profiling floats and histor-
 506 ical oceanographic data and found no increase in the tilt of isopycnals across
 507 the ACC in spite of the observed significant intensification of the South-
 508 ern Ocean westerlies. From these observations, they concluded that both
 509 the ACC transport and the Southern Ocean MOC are insensitive to recent
 510 changes in wind stress. Results from our simple model experiments suggest
 511 that the lack of observational evidence for changes in isopycnal slope may
 512 mean that the ocean is in a strong restoring limit. If this is the case, then
 513 the residual MOC may have actually changed significantly, although such
 514 change is hard to observe. In contrast, if a large change in isopycnal slope
 515 was detected, this does not necessarily mean that the residual MOC must
 516 change similarly—the ocean may be in a weak restoring limit.

517 For this study, we have chosen to use the idealised model setup of Aber-
 518 nathey et al. (2011) because it provides a simple yet physically-appealing
 519 framework. No topography and fixed stratification imposed at the north-
 520 ern boundary are probably the most severe limitations of this model (see
 521 Abernathey et al. (2011) for detailed discussions). At shorter restoring time
 522 scales, the deepening of the isotherms due to increasing wind stress appears
 523 to be arrested by the sponge layer imposed at the northern boundary (Fig.
 524 9), rendering the mean isothermal slopes less sensitive to wind stress changes.
 525 However, this does not necessarily mean the sensitivity to the surface restor-
 526 ing time scale would be reduced if there were ocean basins to the north of the
 527 channel model. In the ocean, we expect these thermocline depth anomalies

528 on the northern flank of the ACC to propagate to the rest of the ocean via
529 boundary and Rossby wave adjustment processes and to be absorbed by the
530 vast surface area of ocean basins to the north (e.g. Allison et al., 2011). This
531 implies that the surface restoring time scale in the Southern Ocean may play
532 a role in regulating the depth of the global pycnocline. Efforts are currently
533 underway to include ocean basins further to the north of the channel as well
534 as bottom topography.

535 A major motivation for the present study is the uncertainty associated
536 with the surface restoring time scale owing to the lack of observations. For
537 example, studies based on heat flux data derived from ship and satellite
538 observations suggest that the restoring time scales can vary from less than one
539 month to almost one year in the Southern Ocean, depending on season and
540 location (e.g. Park et al., 2005). In another observation-based study, Zhai and
541 Greatbatch (2006a) found considerable uncertainty and spatial variability of
542 the surface restoring time scale, ranging from a few days in the Gulf Stream
543 region to over several months in the interior of the subtropical gyre. The
544 strong dependence of the Southern Ocean response to wind stress changes
545 on the surface restoring time scale found in the present study points to the
546 importance of accurately estimating the effect of surface turbulent heat fluxes
547 on sea surface temperature anomalies as well as air-sea buoyancy fluxes in
548 general.

549 **Acknowledgements**

550 Numerical model experiments were carried out on the High Performance
551 Computing Cluster supported by the Research and Specialist Computing

552 Support service at the University of East Anglia. We thank Andy Hogg,
553 David Marshall, and two anonymous reviewers for valuable comments.

554 **References**

555 Abernathey, R., Marshall, J., Ferreira, D., 2011. The dependence of Southern
556 Ocean meridional overturning on wind stress. *J. Phys. Oceanogr.* 41, 2261–
557 2278.

558 Allison, L. C., Johnson, H. L., Marshall, D. P., 2011. Spin-up and adjustment
559 of the Antarctic Circumpolar Current and global pycnocline. *J. Mar. Res.*
560 69, 167–189.

561 Anderson, R. F., Ali, S., Bradtmiller, L. I., Nielsen, S. H. H., Fleisher, M. Q.,
562 Anderson, B. E., Burckle, L. H., 2009. Wind-driven upwelling in the South-
563 ern Ocean and the deglacial rise in atmospheric CO₂. *Science* 323, 1143–
564 1150.

565 Badin, G., Williams, R. G., 2010. On the buoyancy forcing and residual
566 circulation in the Southern Ocean: The feedback from Ekman and eddy
567 transfer. *J. Phys. Oceanogr.* 40, 295–311.

568 Böning, C. W., Dispert, A., Visbeck, M., Rintoul, S. R., Schwarzkopf, F. U.,
569 2008. The response of the Antarctic Circumpolar Current to recent climate
570 change. *Nat. Geosci.* 1, 864–869.

571 Bretherton, F. P., 1982. Ocean climate modeling. *Prog. Oceanogr.* 11, 93–
572 129.

573 Chang, E. K. M., Guo, Y., Xia, X., 2012. CMIP5 multimodel ensemble
574 projection of storm track change under global warming. *J. Geophys. Res.*
575 117.

576 Farneti, R., Delworth, T. L., Rosati, A. J., Griffies, S. M., Zeng, F., 2010.
577 The role of mesoscale eddies in the rectification of the Southern Ocean
578 response to climate change. *J. Phys. Oceanogr.* 40, 1539–1557.

579 Frankignoul, C., 1985. Sea surface temperature anomalies, planetary waves
580 and air-sea feedback in the midlle latitudes. *Rev. Geophys.* 23, 357–390.

581 Fyfe, J. C., Saenko, O. A., 2006. Simulated changes in the extratropical
582 Southern Hemisphere winds and currents. *Geophys. Res. Lett.* 33.

583 Greatbatch, R. J., Zhai, X., Eden, C., Olbers, D., 2007. The possible role in
584 the ocean heat budget of eddy-induced mixing due to air-sea interaction.
585 *Geophys. Res. Lett.* 34.

586 Hallberg, R., Gnanadesikan, A., 2006. The role of eddies in determining the
587 structure and response of the wind-driven southern hemisphere ouverturn-
588 ing: Results from Modeling Eddies in the Southern Ocean (MESO) project.
589 *J. Phys. Oceanogr.* 36, 2232–2252.

590 Haney, R., 1971. Surface thermal boundary condition for ocean circulation
591 models. *J. Phys. Oceanogr.* 1, 241–248.

592 Large, W. G., McWilliams, J. C., Doney, S. C., 1994. Oceanic vertical mixing:
593 A review and a model with a nonlocal boundary layer parmeterization.
594 *Rev. Geophys.* 32, 363–403.

- 595 Marshall, D. P., 1997. Subduction of water masses in an eddying ocean. *J.*
596 *Mar. Res.* 55, 201–222.
- 597 Marshall, D. P., Maddison, J. R., Berloff, P. S., 2012. A framework for param-
598 eterizing eddy potential vorticity fluxes. *J. Phys. Oceanogr.* 42, 539–557.
- 599 Marshall, J., Adcroft, A., Hill, C., Perelman, L., Heisey, C., 1997. A finite-
600 volume, incompressible Navier Stokes model for studies of the ocean on
601 parallel computers. *J. Geophys. Res.* 102, 5753–5766.
- 602 Marshall, J., Radko, T., 2003. Residual-mean solutions for the Antarctic
603 Circumpolar Current and its associated overturning circulation. *J. Phys.*
604 *Oceanogr.* 33, 2341–2354.
- 605 Marshall, J., Speer, K., 2012. Closure of the meridional overturning circula-
606 tion through Southern Ocean upwelling. *Nature Geo.* 5, 171–180.
- 607 Meredith, M. P., Hogg, A. M., 2006. Circumpolar response of Southern Ocean
608 eddy activity to a change in the Southern Hemisphere Mode. *Geophys. Res.*
609 *Lett.* 33.
- 610 Meredith, M. P., Naveira Garabato, A. C., Hogg, A. M., Farneti, R., 2012.
611 Sensitivity of the overturning circulation in the Southern Ocean to decadal
612 changes in wind forcing. *J. Climate* 25, 99–110.
- 613 Morrison, A. K., Hogg, A. M., 2013. On the relationship between Southern
614 Ocean overturning and ACC transport. *J. Phys. Oceanogr.* 43, 140–148.
- 615 Morrison, A. K., Hogg, A. M., Ward, M. L., 2011. Sensitivity of the Southern

616 Ocean overturning circulation to surface buoyancy forcing. *Geophys. Res.*
617 *Lett.* 38.

618 Munday, D. R., Allison, L. C., Johnson, H. L., Marshall, D. P., 2011. Re-
619 mote forcing of the Antarctic Circumpolar Current by diapycnal mixing.
620 *Geophys. Res. Lett.* 38.

621 Munday, D. R., Johnson, H. L., Marshall, D. P., 2013. Eddy saturation of
622 equilibrated circumpolar currents. *J. Phys. Oceanogr.* 43, 507–532.

623 Munday, D. R., Zhai, X., 2013. Modulation of eddy kinetic energy, temper-
624 ature variance, and eddy heat fluxes by surface buoyancy forcing. *Ocean*
625 *Modell.* 62, 27–38.

626 Park, S., Deser, C., Alexander, M. A., 2005. Estimation of the surface heat
627 flux response to sea surface temperature anomalies over the global oceans.
628 *J. Climate* 18, 4582–4599.

629 Rintoul, S., Hughes, C., Olbers, D., 2001. The Antarctic Circumpolar Cur-
630 rent system. In: Sielider, G., Church, J., Gould, J. (Eds.), *Ocean Circula-*
631 *tion and Climate*. Academic Press, pp. 171–302.

632 Shuckburgh, E., Maze, G., Ferreira, D., Marshall, J., Jones, H., Hill, C.,
633 2011. Mixed layer lateral eddy fluxes mediated by air-sea interaction. *J.*
634 *Phys. Oceanogr.* 41, 130–144.

635 Smith, K. S., 2007. The geography of linear baroclinic instability in Earth’s
636 oceans. *J. Mar. Res.* 65, 655–683.

637 Solomon, S., Qin, D., Manning, M., Marquis, M., Averyt, K., Tignor, M.
638 M. B., Miller, H. L., Chen, Z. (Eds.), 2007. *Climate Change 2007: The*
639 *Physical Science Basis*. Cambridge University Press, p. 996 pp.

640 Straub, D., 1993. On the transport and angular momentum balance of chan-
641 nel models of the Antarctic Circumpolar Current. *J. Phys. Oceanogr.* 23,
642 776–783.

643 Toggweiler, J. R., Russell, J., 2008. Ocean circulation in a warming climate.
644 *Nature* 451, 286–288.

645 Viebahn, J., Eden, C., 2010. Towards the impact of eddies on the response
646 of the Southern Ocean to climate change. *Ocean Modell.* 34, 150–165.

647 Visbeck, M., Marshall, J., Haine, T., Spall, M., 1997. On the specification of
648 eddy transfer coefficients in coarse resolution ocean circulation models. *J.*
649 *Phys. Oceanogr.* 27, 381–402.

650 Walin, G., 1982. On the relation between sea-surface heat flow and thermal
651 circulation in the ocean. *Tellus* 34, 187–195.

652 Watson, A. J., Naveira Garabato, A. C., 2006. The role of Southern Ocean
653 mixing and upwelling in glacial-interglacial atmospheric CO₂ change. *Tel-*
654 *lus* 58, 73–87.

655 Zhai, X., 2013. On the wind mechanical forcing of the ocean general circula-
656 tion. *J. Geophys. Res.* 118, 6561–6577.

657 Zhai, X., Greatbatch, R. J., 2006a. Inferring eddy-induced diffusivity for heat
658 in the surface mixed layer using satellite data. *Geophys. Res. Lett.* 33.

- 659 Zhai, X., Greatbatch, R. J., 2006b. Surface eddy diffusivity for heat in a
660 model of the northwest Atlantic Ocean. *Geophys. Res. Lett.* 33.
- 661 Zhai, X., Johnson, H. L., Marshall, D. P., Wunsch, C., 2012. On the wind
662 power input to the ocean general circulation. *J. Phys. Oceanogr.* 42, 1357–
663 1365.